

# Exploiting deterministic algorithms to perform global sensitivity analysis of continuous-time Markov chain compartmental models with application to epidemiology

Henri Mermoz KOUYE<sup>(1)</sup>, Gildas MAZO<sup>(1)</sup>, Clémentine PRIEUR<sup>(2)</sup>  
and Elisabeta VERGU<sup>(1,†)</sup>

<sup>(1)</sup>Univ. Paris-Saclay, INRAE, MaIAGE, 78350, Jouy-en-Josas, France

<sup>(2)</sup>Univ. Grenoble Alpes, CNRS, Inria, Grenoble INP, LJK, 38000, Grenoble, France

<sup>(†)</sup>E. Vergu died on May 13, 2023, during the writing of this paper

March 20, 2024

## Abstract

In this paper, we propose a generic approach to perform global sensitivity analysis (GSA) for compartmental models based on continuous-time Markov chains (CTMC). This approach enables a complete GSA for epidemic models, in which not only the effects of uncertain parameters such as epidemic parameters (transmission rate, mean sojourn duration in compartments) are quantified, but also those of intrinsic randomness and interactions between the two. The main step in our approach is to build a deterministic representation of the underlying continuous-time Markov chain by controlling the latent variables modeling intrinsic randomness. Then, model output can be written as a deterministic function of both uncertain parameters and controlled latent variables, so that it becomes possible to compute standard variance-based sensitivity indices, e.g. the so-called Sobol' indices. However, different simulation algorithms lead to different representations. We exhibit in this work three different representations for CTMC stochastic compartmental models and discuss the results obtained by implementing and comparing GSAs based on each of these representations on a SARS-CoV-2 epidemic model.

**Keywords:** stochastic compartmental models, continuous-time Markov chains, epidemic models, global sensitivity analysis, uncertainty quantification.

## 1 Introduction

In epidemiology, stochastic compartmental models facilitate the prediction and understanding of spreads of infectious diseases in a host population, such as humans,

animals, or plants. The outputs of those models depend on numerous uncertain parameters such as transmission rate, mean sojourn duration in each compartment or transition probabilities. The aim of sensitivity analysis is to identify, among these parameters, the ones which have the greater impact on the infection spread [Hanthanan Arachchilage et al., 2023, Goel et al., 2023, Massard et al., 2022]. This is useful, e.g., to elaborate efficient control strategies [Ngonghala et al., 2015, Yang et al., 2016] or perform models comparison [Torii et al., 2023]. In the following, we are interested in the global sensitivity analysis (GSA) of stochastic compartmental models used in epidemiology [Courcoul et al., 2011]. We focus on GSA rather than local sensitivity analysis, as the former is better adapted to nonlinear models.

Compartmental models [Brauer, 2008] consist in dividing the host population into compartments, each containing individuals with a similar health status. Health statuses of individuals change over time. Transitions between compartments strongly depend on the individuals' characteristics or the patterns of contacts between them. While in large populations randomness due to individual-to-individual variability averages out, it has a large impact on the transmission process for small populations [Britton, 2009, Bittihn and Golestanian, 2020]. Because they incorporate stochastic effects related to biological or contact events, stochastic compartmental models are used to analyze thoroughly the outbreak of infectious diseases. Throughout, we thus focus on stochastic models, and, more precisely, on continuous-time Markov chains (CTMC). CTMCs assume that inter-event times are distributed according to exponential distributions.

GSA aims at determining the extent to which the variability of an input parameter or of a set of input parameters affects the variability of the model's output (see, e.g., Saltelli et al. [2000], Marino et al. [2008]). Performing GSA for stochastic models is more complex as the model output is tainted with two sources of uncertainty: the intrinsic randomness of the model and the uncertainty on the model parameters (such as mean sojourn duration in each compartment, transmission rate and others). So far, different paradigms have been introduced in the literature for sensitivity analysis of stochastic models.

To do GSAs of stochastic models, a pragmatic approach consists in performing the analysis on both the expectation and the variance of the model output conditionally on the uncertain parameters. Intrinsic randomness is thereby considered as noise and is smoothed by the average. The stochastic model is thus reduced to two deterministic models, for which it is possible to estimate sensitivity indices of the uncertain parameters, such as Sobol' indices [Sobol', 1993]. This approach is often used in practice in various applications, for instance in: Courcoul et al. [2011] to identify key parameters of a model describing the spread of an animal disease in a cattle herd; Rimbaud et al. [2018] for a model describing the spatio-temporal spread of plant pathogens; Richard et al. [2021] for a SARS-CoV-2 spread model; Cristancho Fajardo et al. [2021] for a theoretical metapopulation model. However, such an approach can suffer from inconsistent conclusions. Since GSA is performed separately on the conditional mean and conditional variance, a parameter

can appear to be important for a quantity and not for the other one. Moreover, it may be difficult to efficiently estimate first order Sobol' indices for the conditional mean, as this requires a fine trade-off between explorations and repetitions [Mazo, 2021]. Often, to avoid computational burdens, GSA is performed on meta-models. In Marrel et al. [2012], the conditional mean and variance are emulated by a joint Gaussian process-based model. In Étoré et al. [2020], the conditional mean or the mean exit time from any compact domain are emulated by polynomial chaos. A second approach, which avoids the loss of information induced by averaging over intrinsic randomness, has been introduced by Hart et al. [2017]. In this latter paper, the authors interpret the Sobol'-Hoeffding decomposition (see, e.g., Hoeffding [1948], Sobol' [1993]) as a random decomposition, where the randomness is inherited from the intrinsic randomness of the model. From this decomposition they obtain Sobol' indices (variance-based sensitivity indices) which are themselves random variables. More recently, a different point of view was adopted (see, e.g., Fort et al. [2021], Veiga [2021]). Stochastic models as interpreted as deterministic models with outputs taking values in some set of probability distributions. Sensitivity indices that measure the sensitivity of the output probability distribution to variations of the input parameter values are defined. Finally, another path to handle sensitivity analysis of stochastic models consists in emulating the output probability distribution (see, e.g., Zhu and Sudret [2021, 2023]).

However, none of the aforementioned approaches enables the possibility of doing a complete GSA, in which not only the effects of the uncertain parameters are quantified, but also those of intrinsic randomness and the interactions between the two. The problem of performing a complete GSA for stochastic models is tackled, e.g., in Le Maître and Knio [2015], Jimenez et al. [2017], Navarro Jimenez et al. [2016]. In these papers, model outputs are simulated from a stochastic algorithm. Then the approach consists in reinterpreting this stochastic algorithm as a deterministic one with an augmented set of inputs comprising both the uncertain parameters and the latent variables controlling intrinsic randomness, thus allowing for the application of standard GSA tools to the deterministic algorithm defined in the augmented input space.

There exist different algorithms to simulate a CTMC. To perform complete GSAs of CTMC compartmental models, therefore, we investigate three exact simulation algorithms. The first, Gillespie Direct Method algorithm [Gillespie, 1976], is the most common in epidemiology. However this algorithm does not allow us to separate and control the different types of transitions in the model. Thus we consider two other representations based respectively on Gillespie First Reaction Method [Gillespie, 1976] and Modified Next Reaction Method [Anderson, 2007]. The latter was used for doing a complete GSA of reaction networks in Navarro Jimenez et al. [2016]. The underlying idea of Modified Next Reaction Method is a random time change introduced in Ethier and Kurtz [1986].

Each of the above simulation algorithms leads to a distinct deterministic representation of the same stochastic model. But there is no reason for the results of the corresponding sensitivity analyses to coincide. In the present paper, we aim

at exploring this issue, which to the best of our knowledge has not been tackled in the literature yet. Once this issue has been discussed in the general framework of sensitivity analysis of stochastic models, we investigate which representations can be introduced for CTMC compartmental models. We discuss the choice of representations, which depends on the type of results we are interested in.

The paper is organized as follows. We first introduce in Section 2.1 the class of compartmental models we are interested in, whose mathematical formulation is a CTMC. Then in Section 2.2 we recall the definition of variance-based Sobol' indices [Sobol', 1993] for sensitivity analysis of deterministic models. Then we explain in Section 3 how it is possible to perform a complete GSA of a stochastic model if we can represent it as a deterministic function of controlled latent variables (modeling the intrinsic randomness) and uncertain parameters. We also exhibit in Section 3.2 a toy example showing that such a representation is not unique and that GSA results depend on the choice of representations. Thus GSA results have to be interpreted with caution. In Section 4, we propose three deterministic representations for CTMC stochastic compartmental models based on three different simulation algorithms. We illustrate our approach in Section 5 by considering a parsimonious SARS-CoV-2 spread model as a case study. We compare and discuss the GSA results obtained with the different representations presented in Section 4. Finally the main conclusions of our study are recalled in Section 6.

## 2 Preliminaries

We first recall in Section 2.1 the definition of CTMC stochastic compartmental models we are interested in. Then in Section 2.2 we recall the definition of variance-based Sobol' indices [Sobol', 1993] used for GSA in the framework of deterministic models.

### 2.1 CTMC stochastic compartmental models

Consider a finite, closed (i.e. of constant size over time) population in which each individual has a health status (susceptible, infectious, and so on) evolving over time. The set of all possible health statuses is denoted by  $\mathbf{V}$ . Since those health statuses induce a partition of the whole population at any given time, the elements of  $\mathbf{V}$  are also called compartments. Every time an individual changes compartments, we say that a transition occurs. Only certain types of transitions can occur. Let  $\mathbf{E}$  denote the set of all possible types of transitions. By definition, for  $\alpha, \beta \in \mathbf{V}$ , an individual can move from  $\alpha$  to  $\beta$  if  $(\alpha, \beta) \in \mathbf{E}$ . The pair  $(\mathbf{V}, \mathbf{E})$  can be identified with a directed graph where  $\mathbf{V}$  is the set of nodes and  $\mathbf{E}$  is the set of arrows connecting the compartments between which the individuals can move. Assuming an ordering of the compartments has been chosen, let us identify the set  $\mathbf{E}$  with a subset of  $\mathbb{R}^{|\mathbf{V}|}$  as follows: with each  $(\alpha, \beta) \in \mathbf{E}$ , associate the vector of length  $|\mathbf{V}|$  with components equal to zero except at the positions corresponding to  $\alpha$  and

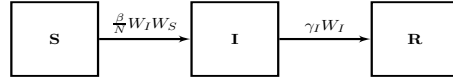
$\beta$ , where the components are  $-1$  and  $1$ , respectively. The elements of  $\mathbf{E}$  seen as a subset of  $\mathbb{R}^{|\mathbf{V}|}$  are called transition vectors.

For every  $\alpha \in \mathbf{V}$  and a vector of epidemic parameters  $\theta \in \Theta \subset \mathbb{R}^d$ , let  $W_\alpha^\theta(t)$  be the number of individuals in compartment  $\alpha$  at time  $t$ . Since the population is closed, we have that  $\sum_{\alpha \in \mathbf{V}} W_\alpha^\theta(t)$  is constant over time. Denote by  $W^\theta = (W_\alpha^\theta)_{\alpha \in \mathbf{V}}$  the stochastic process that describes the whole population over time. It is assumed that  $W^\theta$  is a continuous-time Markov chain with state space  $\mathcal{E} \subset \mathbb{N}^{|\mathbf{V}|}$  and positive rate functions  $g_{\mathbf{u}}(\theta, \xi)$ ,  $\mathbf{u} \in \mathbf{E}$ ,  $\xi \in \mathcal{E}$ , given by

$$\Pr(W^\theta(t+s) = \xi + \mathbf{u} | W^\theta(t) = \xi) = g_{\mathbf{u}}(\theta, \xi)s + o(s) \text{ as } s \rightarrow 0.$$

The initial state  $W^\theta(0) =: \xi_0 \in \mathcal{E}$  is supposed to be fixed. A description of the CTMC of the classical SIR model is given in Example 1.

**Example 1.** *The classical SIR model is described as follows. There are three compartments  $\mathbf{V} = \{S, I, R\}$  and two types of transitions: infection  $(S, I)$  and removal  $(I, R)$  so that  $\mathbf{E} = \{(S, I), (I, R)\} = \{(-1, 1, 0), (0, -1, 1)\}$ . Infection is characterized by the transition vector  $\mathbf{u}_{S,I} = (-1, +1, 0)$  and the rate function  $g_{S,I} = \frac{\beta}{N} W_I W_S$ , where  $\beta$  is some parameter and  $N$  is the total size of the population. Removal has transition vector  $\mathbf{u}_{I,R} = (0, -1, +1)$  and rate function  $g_{I,R} = \gamma W_I$ , where  $\gamma$  is some parameter. The vector of parameters is  $\theta = (\beta, \gamma)$ . The graph of the SIR model is given below:*



## 2.2 Global Sensitivity Analysis

In this section, we first recall the definition of variance-based Sobol' sensitivity indices introduced in Sobol' [1993] for deterministic models with scalar outputs. Following the paradigm of GSA, we model uncertain inputs by a random vector of independent components  $\mathbf{X} = (X_1, \dots, X_m)$ . Let  $E_1, \dots, E_m$  be subsets of  $\mathbb{R}$  and  $f_1 : E_1 \times \dots \times E_m \rightarrow \mathbb{R}$  be some function such that  $\mathbb{E}(f_1(\mathbf{X})^2) < +\infty$ . Then first-order and total Sobol' indices (see, e.g., Sobol' [1993], Homma and Saltelli [1996]) of the output  $Y = f_1(\mathbf{X})$  associated with input  $X_j, j = 1, \dots, m$ , are respectively defined as:

$$S_{X_j} = \frac{\text{Var}(\mathbb{E}[Y | X_j])}{\text{Var}(Y)}, \quad (1)$$

$$\begin{aligned} S_{X_j}^{\text{tot}} &= 1 - \frac{\text{Var}(\mathbb{E}[Y | X_1, \dots, X_{j-1}, X_{j+1}, \dots, X_m])}{\text{Var}(Y)} \\ &=: 1 - \frac{\text{Var}(\mathbb{E}[Y | \mathbf{X}_{-j}])}{\text{Var}(Y)}. \end{aligned} \quad (2)$$

The definition of first-order and total Sobol' indices can be extended to models with vectorial or functional outputs (see, e.g., [Lamboni et al. \[2011\]](#), [Gamboa et al. \[2014\]](#)). Let  $(Y_1, \dots, Y_p) := f_2(X_1, \dots, X_m)$  be a vectorial output where  $f_2 : E_1 \times \dots \times E_m \rightarrow \mathbb{R}^p$  is some function and  $\mathbb{E}(\|Y\|^2) < +\infty$ , with  $\|\cdot\|$  denoting the Euclidean norm on  $\mathbb{R}^p$ . Aggregated first-order and total Sobol' indices are defined as:

$$S_{X_j} = \frac{\sum_{k=1}^p \text{Var}(Y_k) S_{X_j,k}}{\sum_{k=1}^p \text{Var}(Y_k)}, \quad (3)$$

$$S_{X_j}^{\text{tot}} = \frac{\sum_{k=1}^p \text{Var}(Y_k) S_{X_j,k}^{\text{tot}}}{\sum_{k=1}^p \text{Var}(Y_k)}, \quad (4)$$

where  $S_{X_j,k}$  and  $S_{X_j,k}^{\text{tot}}$  are the first-order and total Sobol' indices of the scalar output  $Y_k$  associated with the input  $X_j$ , for  $k = 1, \dots, p$  and  $j = 1, \dots, m$ . If the output of the model of interest is a function of time, it can be reduced to a vectorial output through discretization of time. Then aggregated first-order and total Sobol' indices can be computed using (3) and (4), where the output components  $Y_k$  would be the values of the function at the time points of the discretization. Also first-order and total indices defined in Equations (1) and (2) can be computed at each time point of the discretization in order to obtain dynamics of Sobol' indices.

### 3 Complete GSA for stochastic models

In this section we aim at quantifying partial variances due on one hand to uncertain parameters or groups of uncertain parameters, on the other hand to intrinsic randomness, and finally to the interaction between arbitrary groupings of uncertain parameters and intrinsic randomness. We call this a complete GSA. A strategy to achieve this aim requires controlling the latent variables modeling intrinsic randomness.

#### 3.1 Deterministic representations of stochastic models

Let  $Y^\theta$  denote the random output of some stochastic model with parameters  $\theta \in \Theta \subset \mathbb{R}^d$ . For instance,  $Y^\theta$  might be the stochastic process  $W^\theta$  introduced in Section 2.1, or any scalar (or vectorial) quantity of interest defined as a functional of the process  $W^\theta$ . Note that distinct values of the parameters encoded in  $\theta$  correspond to distinct epidemiological patterns. We thus consider the collection  $\{Y^\theta, \theta \in \Theta\}$  and assume mutual independence between its members.

As in Section 2.2, uncertain parameters are modeled by a random vector  $\mathbf{X} = (X_1, \dots, X_d)$  with independent components. In addition, it is assumed that  $\mathbf{X}$  is independent of  $\{Y^\theta, \theta \in \Theta\}$ . The pair  $(\mathbf{X}, Y^{\mathbf{X}})$  represents the input/output pair that an external observer would see should they draw uncertain parameters at random. The object  $Y^\theta$  is then the output observed conditionally on  $\mathbf{X} = \theta$ .

It is important to note that in  $Y^{\mathbf{X}}$  there are two sources of variability (and hence uncertainty): the one coming from the uncertainty of the parameters (that is, modeled by vector  $\mathbf{X}$ ), and the one coming from the intrinsic randomness of the stochastic model (that is, for a fixed  $\theta$  the variability in  $Y^\theta$ ). A complete GSA aims at separating these two sources of uncertainty and quantifying interactions between both.

To achieve this aim, it is necessary to control the latent variables modeling intrinsic randomness. More precisely, we aim at finding a function  $f$  and a latent or a set of latent variables  $Z$ , independent of  $\mathbf{X}$ , such that the probability distributions of  $Y^\theta$  and  $f(\theta, Z)$  coincide. Since  $\mathbf{X}$  is independent of  $Z$  and  $Y^\theta$ , we immediately have that the input/output pairs  $(\mathbf{X}, Y^{\mathbf{X}})$  and  $(\mathbf{X}, f(\mathbf{X}, Z))$  are equal in distribution. The pair  $(f, Z)$  is called a *deterministic representation* (or simply a representation) of the stochastic model  $Y^\theta$ . Often, the function  $f$  is the function induced by a (deterministic) algorithm which, if the inputs of that algorithm were drawn from the right distribution, would produce an output statistically equal to the given stochastic model.

From the viewpoint of GSA, one advantage of constructing a deterministic representation of a stochastic model is that standard methods of GSA for deterministic models can be applied straightforwardly. For instance, we can compute first-order and total Sobol' indices by letting  $m = d + 1$  and  $X_{d+1} = Z$  in (1) and (2) (or in (3) and (4) if the output is vectorial or functional).

In general, there is no unique deterministic representation of a stochastic model. The set of latent variables modeling intrinsic randomness  $Z$  and the function  $f$  may vary from one representation to the other. More precisely, if  $Y^\theta$  is a stochastic model and  $(f, Z)$  a representation of it, there may exist another representation  $(\tilde{f}, \tilde{Z})$  of  $Y^\theta$  such that the laws of  $(\mathbf{X}, \tilde{f}(\mathbf{X}, \tilde{Z}))$  and  $(\mathbf{X}, f(\mathbf{X}, Z))$  coincide. (Here the probability distribution of  $\tilde{Z}$  may be different from that of  $Z$ .) An example of a toy stochastic model with two different representations is provided in Example 2 below.

**Example 2.** Let  $Z \sim \mathcal{U}([0, 1])$  independent of  $(\mathbf{X}, Z_1, Z_2) \sim \mathcal{N}(0_{\mathbb{R}^3}, \text{Id}_3)$ . Consider the stochastic model  $Y^\theta \sim \mathcal{N}(\theta, 1)$ . This model can be represented by using  $f(\theta, Z_1, Z_2) = \theta + \frac{1}{\sqrt{2}}(Z_1 + Z_2)$  or  $\tilde{f}(\theta, Z) = \theta + \Phi^{-1}(Z)$ , where  $\Phi$  is the cumulative distribution function of the standard normal distribution.

### 3.2 How does a complete GSA depend on the chosen representation?

As different representations can be exhibited for a same stochastic model, we can wonder how the choice of representations affects GSA results. Let us consider  $(f, Z)$  and  $(\tilde{f}, \tilde{Z})$  two distinct representations of a same stochastic model with uncertain parameters  $\mathbf{X} = (X_1, \dots, X_d)$  and output  $Y^{\mathbf{X}}$ . We say that an index  $S_{X_j}$  is *representation free* if  $S_{X_j}(f, Z) = S_{X_j}(\tilde{f}, \tilde{Z})$ , where here  $S_{X_j}(f, Z)$  and  $S_{X_j}(\tilde{f}, \tilde{Z})$  denote the values of the index  $S_{X_j}$  based on the representations  $(f, Z)$  and  $(\tilde{f}, \tilde{Z})$ , respectively.

**Proposition 1.** *First-order Sobol' indices associated with uncertain parameters are representation free.*

*Proof.* From Section 3 we know that

$$(\mathbf{X}, Y^{\mathbf{X}}) \sim (\mathbf{X}, f(\mathbf{X}, Z)) \sim (\mathbf{X}, \tilde{f}(\mathbf{X}, \tilde{Z})). \quad (5)$$

Thus, for  $j = 1, \dots, d$ , we have almost surely the following equality:

$$\mathbb{E}[f(\mathbf{X}, Z) \mid X_j] = \mathbb{E}[\tilde{f}(\mathbf{X}, \tilde{Z}) \mid X_j]$$

from which we deduce, using (1), that  $S_{X_j}(f, Z) = S_{X_j}(\tilde{f}, \tilde{Z})$ , where here  $S_{X_j}(f, Z)$  and  $S_{X_j}(\tilde{f}, \tilde{Z})$  denote the first-order Sobol' indices associated with  $X_j$  based on  $(f, Z)$  and  $(\tilde{f}, \tilde{Z})$ , respectively.  $\square$

**Proposition 2.** *Total Sobol' indices associated with intrinsic randomness are representation free.*

*Proof.* Put  $X'_j = X_j$ ,  $j = 1, \dots, d$ ,  $X'_{d+1} = Z$  and  $m = d + 1$  so that  $\mathbf{X}' := (X'_1, \dots, X'_m) = (\mathbf{X}, Z)$ . From (5), we deduce the following almost sure equality:

$$\mathbb{E}[f(\mathbf{X}, Z) \mid \mathbf{X}'_{-m}] = \mathbb{E}[f(\mathbf{X}, Z) \mid \mathbf{X}] = \mathbb{E}[\tilde{f}(\mathbf{X}, \tilde{Z}) \mid \mathbf{X}] = \mathbb{E}[\tilde{f}(\mathbf{X}, \tilde{Z}) \mid \mathbf{X}'_{-m}],$$

from which we deduce, using (2), that the total Sobol' indices  $S_Z^{\text{tot}}(f, Z)$  and  $S_{\tilde{Z}}^{\text{tot}}(\tilde{f}, \tilde{Z})$  associated with intrinsic randomness and based respectively on  $(f, Z)$  and  $(\tilde{f}, \tilde{Z})$  are equal.  $\square$

**Proposition 3.** *First-order Sobol' indices associated with intrinsic randomness and total Sobol' indices associated with uncertain parameters depend on the choice of representations in general.*

To show that Proposition 3 is true, it suffices to exhibit an example where two distinct representations lead to distinct first-order Sobol' indices associated with intrinsic randomness and distinct total Sobol' indices associated with uncertain parameters. Before giving the example, let us give some intuition behind Proposition 3. Note that the random variables  $\mathbb{E}[f(\mathbf{X}, Z) \mid (\mathbf{X}_{-j}, Z)]$  and  $\mathbb{E}[\tilde{f}(\mathbf{X}, \tilde{Z}) \mid (\mathbf{X}_{-j}, \tilde{Z})]$  have different probability distributions in general. Indeed, since  $(f, Z) \neq (\tilde{f}, \tilde{Z})$ , the way each function  $f$  or  $\tilde{f}$  combines its (set of) latent variable(s)  $Z$  with input  $X_j$  to generate outputs may differ. Thus there is no reason for total Sobol' indices associated with uncertain parameters to be representation free. Also, there is no reason for the random variables  $\mathbb{E}[f(\mathbf{X}, Z) \mid Z]$  and  $\mathbb{E}[\tilde{f}(\mathbf{X}, \tilde{Z}) \mid \tilde{Z}]$  to have the same probability distributions and hence the first-order Sobol' index associated with intrinsic randomness to be representation free. This is illustrated on the toy Example 3 below.

**Example 3.** Let  $X$  be a random variable independent of  $Z$  and  $\tilde{Z}$  where  $Z$  and  $\tilde{Z}$  are i.i.d. under  $\mathcal{N}(0, 1)$ . Define two functions:  $f(X, Z) = XZ$  and  $\tilde{f}(X, \tilde{Z}) = X^2\tilde{Z}$ . If  $X$  is distributed such that  $\mathbb{P}(X = -1) = \mathbb{P}(X = 1) = \frac{1}{2}$  then  $(X, f(X, Z)) \sim (X, \tilde{f}(X, \tilde{Z}))$ . Thus,  $(f, Z)$  and  $(\tilde{f}, \tilde{Z})$  represent the same stochastic model but:  $\mathbb{E}[f(X, Z) | Z] = 0$  while  $\mathbb{E}[\tilde{f}(X, \tilde{Z}) | \tilde{Z}] = \tilde{Z}$ . Simple calculations then lead to  $S_Z(f, Z) = 0$  while  $S_{\tilde{Z}}(\tilde{f}, \tilde{Z}) = 1$ . Total Sobol' indices associated to  $X$  can easily be deduced:  $S_X^{\text{tot}}(f, Z) = 1 - S_Z(f, Z) = 1$  and  $S_X^{\text{tot}}(\tilde{f}, \tilde{Z}) = 1 - S_{\tilde{Z}}(\tilde{f}, \tilde{Z}) = 0$ .

We conclude from this section that intrinsic randomness can be modeled in different manners. GSA results naturally depend on the modeling choice. Different modelings bring different insights. Thus the choice of representations must be made with caution, in consultation with epidemiologists. We discuss this point further on a SARS-CoV-2 spread model in Section 5. In the following section, we exhibit different meaningful representations for CTMC stochastic compartmental models, based on different simulation algorithms.

## 4 Deterministic representations for CTMC stochastic compartmental models

Following Section 2.1, let  $W^\theta$  be a CTMC stochastic compartmental model with uncertain parameters  $\theta$ . As explained in Section 3, we wish to rewrite the trajectories of  $W^\theta$  as a function of the uncertain parameters and some set of latent variables so as to perform a complete GSA. Based on three different exact simulation algorithms, we propose in this section three different deterministic representations for the same generic CTMC stochastic compartmental model.

One of the first and most basic procedure to simulate the trajectory of a CTMC is as follows. Given that the chain is at some state  $W^\theta(s) = \xi$  at time  $s$ , the holding time until the next jump is distributed as an exponential random variable with parameter  $\sum_{\mathbf{u} \in \mathbf{E}} g_{\mathbf{u}}(\theta, \xi)$  and then the chain moves to state  $\xi + \mathbf{u}$  with probability  $g_{\mathbf{u}}(\theta, \xi) / \sum_{\mathbf{u} \in \mathbf{E}} g_{\mathbf{u}}(\theta, \xi)$ . See, e.g. Karlin and Taylor [1981] for more details. In epidemiology, this procedure is known as Gillespie Direct Method [Gillespie, 1976].

Algorithm 1 is a slightly modification of Gillespie Direct Method based on pseudo-random number generators  $RG_j$ ,  $j = 1, 2$ . Here each pseudo-random number generator is seen as an infinite sequence of pseudo-random numbers determined by the seed of the generator. Thus, to get a deterministic representation of the stochastic model  $W^\theta$ , we let  $Z$  represent the value of the seed and  $f(\theta, z)$  represent the output of Algorithm 1 for some specific seed value  $Z = z$ . In practice, the seed values are drawn uniformly over a large number of possible seed values.

We remark that the time-marching method of Algorithm 1 does not require the storage of holding times. Instead, the sequence of holding times is determined on the fly using the pseudo random number generator  $RG_1$ . In the same way the sequence of types of transition is determined using the random number generator

$RG_2$ . In practice, the sequences of holding times and types of transition are entirely determined by the seeds initializing the pseudo-random number generators  $RG_j$ ,  $j = 1, 2$ . Identical sequences of holding times and types of transition are produced if the same seeds are used. Compared to other algorithms for simulating CTMCs, the main advantage of Algorithm 1 is its low simulation cost.

Algorithm 1 combines all types of transitions to determine the next holding time and then the associated type of transition. However, interpretation of intrinsic randomness in this case is difficult. To overcome this issue, we introduce Algorithm 2 below, which is a slight modification of Gillespie First Reaction Method using pseudo-random number generators. Contrarily to Algorithm 1, Gillespie First Reaction Method analyzes the various types of transitions separately.

Although Gillespie Direct Method and Gillespie First Reaction Method are the most common simulation algorithms in epidemiology, we will compare their results to those obtained from a last simulation algorithm based on the so-called random-time change representation introduced in Kurtz [1982] (see also Ethier and Kurtz [1986]). More precisely, the random state  $W^\theta(t)$  can be expressed, for every  $t \geq 0$ , through

$$W^\theta(t) = W^\theta(0) + \sum_{\mathbf{u} \in \mathbf{E}} Y_{\mathbf{u}} \left( \int_0^t g_{\mathbf{u}}(\theta, W^\theta(s)) ds \right) \mathbf{u},$$

where  $\{Y_{\mathbf{u}}(t), t \geq 0\}$  are independent unit-rate Poisson processes associated with the types of transition  $\mathbf{u} \in \mathbf{E}$ . Introduced in Navarro Jimenez et al. [2016] as a tool for doing complete GSAs of chemical reaction network models [Le Maître et al., 2015], Algorithm 3 below is a slight modification of the Modified Next Reaction Method proposed by Anderson [2007].

---

**Algorithm 1: Gillespie Direct Method**

---

**Inputs :**  $t_{\text{end}}, \theta, Z := (RG_1, RG_2)$

**Data:**  $\xi_0, \mathbf{E}, \{g_{\mathbf{u}}, \mathbf{u} \in \mathbf{E}\}$

**Output:**  $\{W^\theta(s), s \in [0, t_{\text{end}}]\}$

Initialization:  $s \leftarrow 0, W^\theta(s) \leftarrow \xi_0;$

**while**  $s < t_{\text{end}}$  **do**

$\Sigma \leftarrow \sum_{\mathbf{u} \in \mathbf{E}} g_{\mathbf{u}}(\theta, W^\theta(s));$

    Take  $r_1$  from  $RG_1;$

$\Delta \leftarrow -\log(r_1)/\Sigma;$

**for**  $\mathbf{u} \in \mathbf{E}$  **do**

$p_{\mathbf{u}} \leftarrow g_{\mathbf{u}}(\theta, W^\theta(s)) / \Sigma;$

**end**

    Divide the interval  $(0, 1)$  into  $|\mathbf{E}|$  sub-intervals of length  $p_{\mathbf{u}}, \mathbf{u} \in \mathbf{E};$

    Take  $r_2$  from  $RG_2$  and let  $\bar{\mathbf{u}}$  such that  $r_2$  lies within the sub-interval of length  $p_{\bar{\mathbf{u}}};$

$W^\theta(s + \Delta) \leftarrow W^\theta(s) + \bar{\mathbf{u}};$

$s \leftarrow s + \Delta;$

**end**

---

---

**Algorithm 2: Gillespie First Reaction Method**

---

**Inputs :**  $t_{\text{end}}, \theta, Z := \{RG_{\mathbf{u}}, \mathbf{u} \in \mathbf{E}\}$

**Data:**  $\xi_0, \mathbf{E}, \{g_{\mathbf{u}}, \mathbf{u} \in \mathbf{E}\}$

**Output:**  $\{W^\theta(s), s \in [0, t_{\text{end}}]\}$

Initialization:  $s \leftarrow 0, W^\theta(s) \leftarrow \xi_0;$

**while**  $s < t_{\text{end}}$  **do**

**for**  $\mathbf{u} \in \mathbf{E}$  **do**

        Take  $r_{\mathbf{u}}$  from  $RG_{\mathbf{u}};$

$a_{\mathbf{u}} \leftarrow g_{\mathbf{u}}(\theta, W^\theta(s));$

$\Delta_{\mathbf{u}} \leftarrow \frac{-\log(r_{\mathbf{u}})}{a_{\mathbf{u}}}$

**end**

$\bar{\mathbf{u}} \leftarrow \operatorname{argmin}_{\mathbf{u}} \Delta_{\mathbf{u}};$

$\Delta \leftarrow \Delta_{\bar{\mathbf{u}}};$

$W(s + \Delta) \leftarrow W(s) + \bar{\mathbf{u}};$

$s \leftarrow s + \Delta;$

**end**

---

---

**Algorithm 3:** Modified Next Reaction Method

---

**Inputs :**  $t_{\text{end}}, \theta, Z := \{RG_{\mathbf{u}}, \mathbf{u} \in \mathbf{E}\}$

**Data:**  $\xi_0, \mathbf{E}, \{g_{\mathbf{u}}, \mathbf{u} \in \mathbf{E}\}$

**Output:**  $\{W^\theta(s), s \in [0, t_{\text{end}}]\}$

Initialization:

**for**  $\mathbf{u} \in \mathbf{E}$  **do**

    Take  $r_{\mathbf{u}}$  from  $RG_{\mathbf{u}}$ ;

$t_{\mathbf{u}} \leftarrow 0, t_{\mathbf{u}}^+ \leftarrow -\log(r_{\mathbf{u}})$ ;

**end**

$s \leftarrow 0, W^\theta(s) \leftarrow \xi_0$ ;

**while**  $s < t_{\text{end}}$  **do**

**for**  $\mathbf{u} \in \mathbf{E}$  **do**

$a_{\mathbf{u}} \leftarrow g_{\mathbf{u}}(\theta, W(s)); \Delta_{\mathbf{u}} \leftarrow \frac{t_{\mathbf{u}}^+ - t_{\mathbf{u}}}{a_{\mathbf{u}}}$

**end**

$\bar{\mathbf{u}} \leftarrow \operatorname{argmin}_{\mathbf{u}} \Delta_{\mathbf{u}}$ ;

$\Delta \leftarrow \Delta_{\bar{\mathbf{u}}}$ ;

$W(s + \Delta) \leftarrow W(s) + \bar{\mathbf{u}}$ ;

$s \leftarrow s + \Delta$ ;

**for**  $\mathbf{u} \in \mathbf{E}$  **do**

$t_{\mathbf{u}} \leftarrow t_{\mathbf{u}} + a_{\mathbf{u}}\Delta$

**end**

    Take  $r_{\bar{\mathbf{u}}}$  from  $RG_{\bar{\mathbf{u}}}$ ;

$t_{\bar{\mathbf{u}}}^+ \leftarrow t_{\bar{\mathbf{u}}}^+ - \log(r_{\bar{\mathbf{u}}})$ ;

**end**

---

In summary, in this section we introduced three deterministic representations of compartmental models based on CTMCs using three different stochastic simulation algorithms: Gillespie Direct Method (Algorithm 1), Gillespie First Reaction Method (Algorithm 2) and Modified Next Reaction Method (Algorithm 3). As they analyze the various types of transitions separately, Algorithms 2 and 3 are more insightful, but they are also more computationally expensive than Algorithm 1.

The aim of Section 5 will be to implement a complete GSA using each of the above representations on a SARS-CoV-2 spread model. From the theoretical results of Section 3.2, we expect GSA results to differ from one representation to the other, with the take home message that the representation must be chosen with caution and in consultation with epidemiologists.

## 5 Application to a SARS-CoV-2 spread model

Although our approach for a complete GSA of stochastic compartmental models is generic, we propose in this section, as a case study, to do a sensitivity analysis of a parsimonious SARS-CoV-2 spread model, which is a simplified but still realistic version of the model introduced in [Cazelles et al. \[2021\]](#). In this section, we do not

pretend to provide the most suitable model for the propagation of SARS-CoV-2, we rather aim at demonstrating the effectiveness of the approach presented in Section 3 for a complete GSA of stochastic compartmental models. In order to illustrate the statement in Section 3.2 that sensitivity analysis results depend on the deterministic representation chosen for its implementation, we compare the results by using each of Modified Gillespie Direct Method (Algorithm 1), Modified Gillespie First Reaction Method (Algorithm 2) and Modified Next Reaction Method (Algorithm 3) for simulations. Recall that these algorithms have been presented in Section 4. In Section 5.1 we describe the considered SARS-CoV-2 model. Then in Section 5.2 we introduce the quantities of interest and detail our numerical setting for sensitivity analysis. Finally in Section 5.3 we present the results of the sensitivity analyses obtained from the different simulation algorithms of Section 4.

## 5.1 A SARS-CoV-2 spread model

Recall from Section 2 that each process  $W_\alpha^\theta$ ,  $\alpha \in \mathbf{V}$ , counts the number of individuals in compartment  $\alpha$  over time. In this section we let  $\mathbf{V} = \{S, E, A, I, H, R, D\}$ , where the seven compartments represent seven possible health statuses: an individual can be susceptible (S), exposed (E) (i.e. infected but not yet infectious), asymptomatic infectious (A), symptomatic infectious (I), hospitalized (H), recovered (R) or dead (D). There are nine possible types of transition between these compartments, see Figure 1. Note that infection is neglected within hospitals so that hospitalized individuals cannot infect. Moreover, it is assumed that recovered individuals get perfectly immunized so they cannot be susceptible after recovering. The vector of uncertain parameters is given by  $\theta = (\beta, \gamma_E, \gamma_A, \gamma_I, \gamma_H, p_{(E,A)}, p_C, p_{D|C}, p_{(H,D)})$ . The different types of transition and their characteristics (transition vector  $\mathbf{u}$  and associated rate function  $g_{\mathbf{u}}$ ) are described in Table 1.

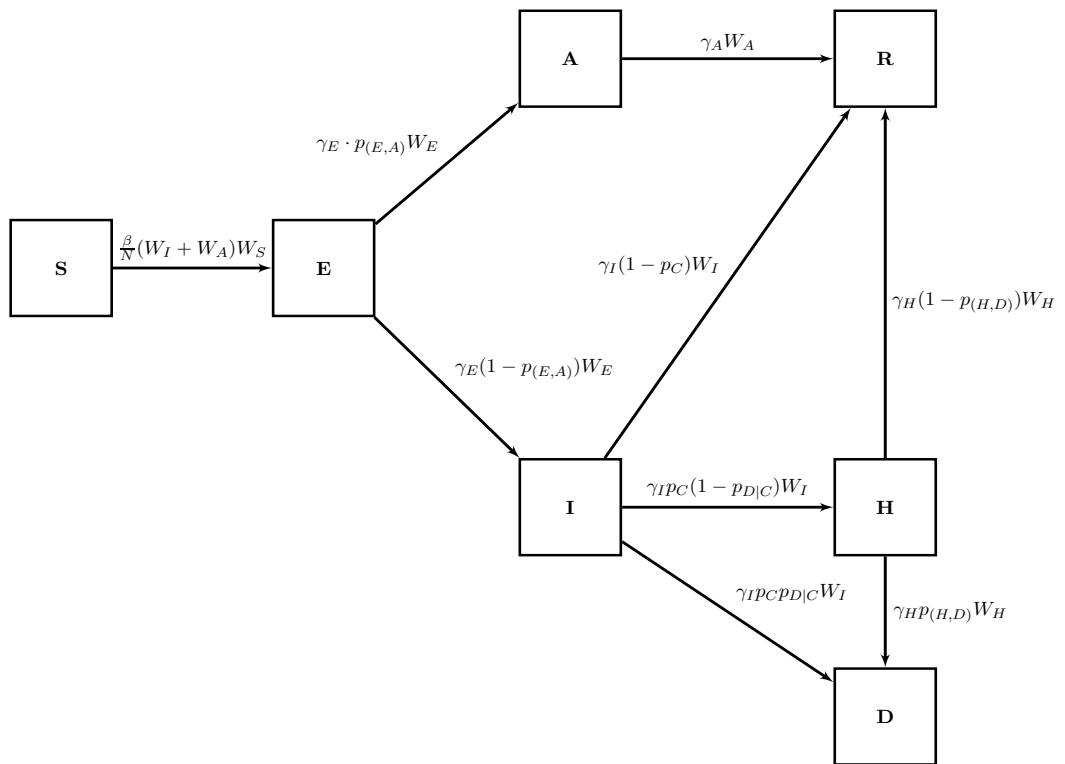


Figure 1: Compartmental model of the spread of SARS-CoV-2. The nodes are the possible health statuses and the arrows connecting them are the possible types of transition. The labels above the arrows are the corresponding rate functions.

Transition	Type	Transition vector $\mathbf{u}$	Rate function $g_{\mathbf{u}}$
$(S, E)$	infection	$(-1, 1, 0, 0, 0, 0, 0)$	$\frac{\beta}{N} \cdot W_S \cdot (W_A + W_I)$
$(E, A)$	asymptomatic infectiousness activation	$(0, -1, +1, 0, 0, 0, 0)$	$\gamma_E \cdot p_{(E,A)} \cdot W_E$
$(E, I)$	symptomatic infectiousness activation	$(0, -1, 0, +1, 0, 0, 0)$	$\gamma_E \cdot (1 - p_{(E,A)}) \cdot W_E$
$(A, R)$	recovery of an asymptomatic	$(0, 0, -1, 0, 0, +1, 0)$	$\gamma_A \cdot W_A$
$(I, R)$	recovery of a symptomatic	$(0, 0, 0, -1, 0, +1, 0)$	$\gamma_I \cdot (1 - p_C) \cdot W_I$
$(I, H)$	hospitalization of a symptomatic	$(0, 0, 0, -1, +1, 0, 0)$	$\gamma_I \cdot p_C \cdot (1 - p_{D C}) \cdot W_I$
$(I, D)$	death of a symptomatic	$(0, 0, 0, -1, 0, 0, +1)$	$\gamma_I \cdot p_C \cdot p_{D C} \cdot W_I$
$(H, R)$	recovery of a hospitalized	$(0, 0, 0, 0, -1, +1, 0)$	$\gamma_H \cdot (1 - p_{(H,D)}) \cdot W_H$
$(H, D)$	death of a hospitalized	$(0, 0, 0, 0, -1, 0, +1)$	$\gamma_H \cdot p_{(H,D)} \cdot W_H$

Table 1: Description of the model transitions between states  $\{S, E, A, I, H, R, D\}$ .

Parameter	Description	Nominal value	Range of variation
$\beta$	transmission rate	2.175	(0.35, 4)
$1/\gamma_E$	mean sojourn duration in $E$	4.5 days	(2, 7)
$1/\gamma_A$	mean sojourn duration in $A$	2 days	(1, 3)
$1/\gamma_I$	mean sojourn duration in $I$	4 days	(3, 5)
$1/\gamma_H$	mean sojourn duration in $H$	9.5 days	(7, 12)
$p_{(E,A)}$	probability for an exposed to become asymptomatic	0.5	(0.3, 0.7)
$p_C$	probability for an individual in compartment $I$ of being in a critical state	0.175	(0.15, 0.2)
$p_{D C}$	probability to die without being hospitalized knowing that the individual is in a critical state	0.175	(0.15, 0.2)
$p_{(H,D)}$	probability for a hospitalized to die	0.0505	(0.001, 0.1)

Table 2: Model parameter nominal values and their range of variation in the sensitivity analysis.

## 5.2 Setting for sensitivity analysis

We consider a population of  $N = 2005$  individuals including five exposed individuals at the start of the epidemic  $t = 0$ , so that the process  $W^\theta$  has the initial state

$$\xi_0 = (W_S(0) = 2000, W_E(0) = 5, \\ W_A(0) = W_I(0) = W_H(0) = W_R(0) = W_D(0) = 0).$$

We focus on two quantities of interest (QoIs). First we consider a scalar QoI, namely the extinction time  $Y_{ext}^\theta$  of the epidemic, defined as the first instant at which there are no exposed (E) nor infectious (A or I) individuals anymore:

$$Y_{ext}^\theta = \inf\{t \geq 0 : W_E^\theta(t) + W_A^\theta(t) + W_I^\theta(t) = 0\}.$$

Note that for all  $\theta \in \Theta$ ,  $Y_{ext}^\theta$  is well-defined, i.e.  $Y_{ext}^\theta < +\infty$ . Indeed, by considering the compartmental model described in Figure 1, after a finite number of transitions, the stochastic process will necessarily reach an absorbing state with empty compartments  $E$ ,  $A$  and  $I$ . We display in Figure 2 two hundred independent realizations of  $Y_{ext}^\theta$  for each of the simulation algorithms of Section 4. The uncertain parameters  $\theta$  were set to the nominal values given in Table 2. These values agree with current knowledge and are considered as plausible (see, e.g., Knock et al. [2021], Da Veiga et al. [2021]). The three boxplots are similar, which was expected since the distributions of the processes returned by each of the three algorithms are the same.

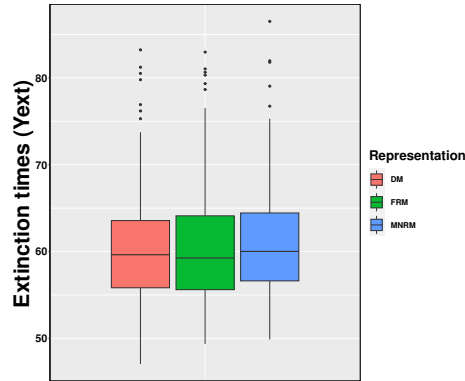


Figure 2: Boxplot of 200 simulations of  $Y_{ext}^\theta$  performed with (left, red) Gillespie Direct Method (middle, green) Gillespie First Reaction (right, blue) Modified Next Reaction algorithm with uncertain parameters  $\theta$  set to the nominal values given in Table 2.

The second QoI we are considering is the dynamic of the number of symptomatic infectious individuals:

$$Y_I^\theta = \{W_I^\theta(t), t \in [0, t_{\text{end}}]\},$$

where  $t_{\text{end}}$  was set to 60. (The process dies out at around that time, see Figure 3.) We display in Figure 3 twenty independent realizations of the process  $Y_I^\theta$  for each of the simulation algorithms of Section 4. The input parameter vector  $\theta$  was set to

the nominal values given in Table 2. The three charts in Figure 3 display similar sample paths for  $Y_I^\theta$ , which was expected since the distribution of the processes returned by each of the three algorithms is the same.

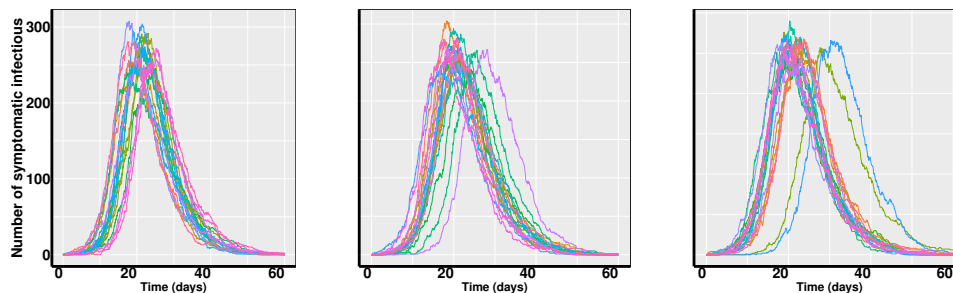


Figure 3: 20 independent realizations of  $t \rightarrow W_I^\theta(t)$ , with  $\theta$  set to nominal values given in Table 2, from (left) Gillespie Direct Method (middle) Gillespie First Reaction (right) Modified Next Reaction algorithm.

As expected, for  $\theta$  fixed to its nominal value, we do not observe on Figure 3 a significant difference in the simulations run with Algorithm 1, 2 or 3.

In practice, simulations are carried out using the R Statistical Software [R Core Team, 2021]. Sensitivity indices are estimated by using the R package `sensitivity` [Iooss et al., 2021]. The function `soboljansen()` is used for total Sobol' index estimation while `sobol2007()` is used for first-order Sobol' index estimation. A priori distributions for model parameters are uniform distributions as described in Table 2 and the a priori for intrinsic randomness is modeled by seeds uniformly distributed in  $\{1, \dots, 10^9\}$ . Sensitivity indices are estimated from two independent designs of  $n = 2000$  input-output samples, where for each sample a trajectory of  $W^\theta$  is simulated through either Algorithm 1, Algorithm 2 or Algorithm 3. As the dimension of the input space is large (at least 7 model parameters plus inputs modeling intrinsic randomness whose number depends on the simulation algorithm), we use Latin Hypercube Sampling (see, e.g., Lin and Tang [2015]). Latin Hypercube Samples are generated by using the R package `DiceDesign` [Dupuy et al., 2015].

### 5.3 Sensitivity analysis results

This section is devoted to the presentation and comparison of sensitivity analysis results obtained for the algorithms presented in Section 4, namely Gillespie Direct Method, Gillespie First Reaction Method and Modified Next Reaction Method. In Section 5.3.1 we present the results for the scalar output of interest, namely the extinction time of the epidemic  $Y_{ext}^\theta$ . Then in Section 5.3.2 we present the sensitivity analysis results for the functional output corresponding to the dynamic of the number of symptomatic infectious individuals  $Y_I^\theta$ . Finally in Section 5.4 we discuss the choice of algorithms, depending on the practitioner's objectives. Recall that in

all the results presented in this section, sensitivity indices were estimated from two independent designs of  $n = 2000$  input-output samples, and the estimation was repeated independently 50 times for the different boxplots.

### 5.3.1 Sensitivity analysis results for $Y_{ext}^\theta$

We display on Figure 4 boxplots of first-order and total Sobol' index estimates.

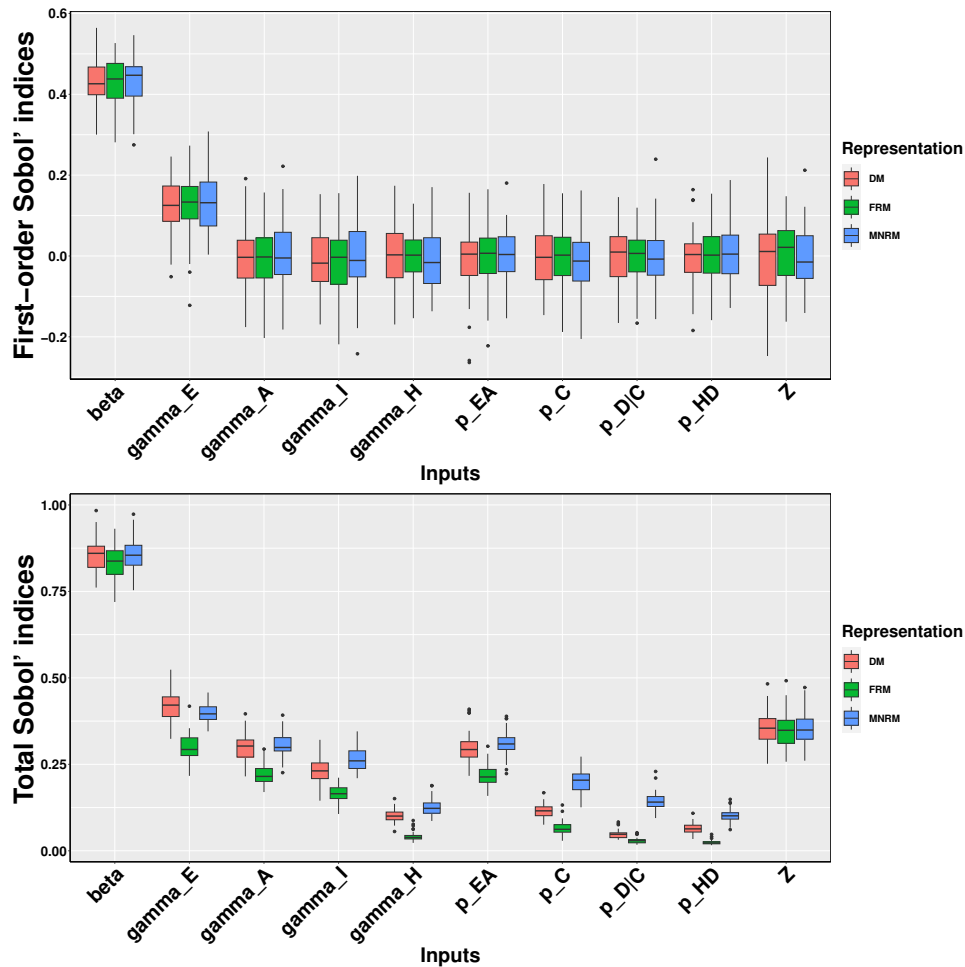


Figure 4: Boxplots of 50 independent estimates of the (top) first-order and (bottom) total Sobol' indices for  $Y_{ext}^\theta$ , each computed with two independent designs of  $n = 2000$  input-output samples, for each simulation algorithm: (red, left) Gillespie Direct Method, (green, middle) Gillespie First Reaction, (blue, right) Modified Next Reaction.

In accordance with the results stated in Section 3.2, we observe on the top of Figure 4 that there are no significant differences between the three algorithms for

the first-order Sobol' index estimates. The only input parameters with a significant first-order effect are  $\beta$  and  $\gamma_E$ . The sum of the first-order index estimates is far below 1 which means that interactions are not negligible. We observe on the bottom of Figure 4 that almost all inputs have a total effect significantly greater than zero. The interaction strength varies from one simulation algorithm to the other. This is due to the fact that the modeling of intrinsic randomness depends on each simulation algorithm. In particular, we observe that the total Sobol' index estimates corresponding to the Modified Next Reaction algorithm are never less than their counterpart computed from the First Reaction Method algorithm. This reflects a stronger interaction with intrinsic random noise for Modified Next Reaction algorithm. Finally, as expected from the theoretical results in Section 3.2, the total index estimates associated with intrinsic randomness do not depend on the chosen simulation algorithm.

### 5.3.2 Sensitivity analysis results for $Y_I^\theta$

Since  $Y_I^\theta$  is a dynamical process, we can consider the sensitivity of the whole trajectory or the sensitivity time by time. In the numerical experiments,  $Y_I^\theta$  is discretized over a regular grid of size 1000 of the interval  $[0, t_{\text{end}}]$ . The sensitivity of the whole trajectory consists of computing estimates of the aggregated sensitivity indices of Section 2.2. These provide a scalar summary for the dynamical evolution of first-order and total Sobol' indices. They are displayed in Figure 5. While the three algorithms show similar first-order Sobol index estimates, they show some significant differences for the total index estimates. We observe that the total index estimates for the uncertain parameters  $\gamma_A, \gamma_I, \gamma_H, p_{E,A}, p_C, p_{D|C}$  and  $p_{H,D}$  are significantly higher for Modified Next Reaction Method, indicating that each of those parameters interacts more with the variable  $Z$ . Then, using Algorithms 2 or 3, it is possible to decompose  $Z$  into components that correspond to the different types of transition. On Figure 6, we plotted first-order and total Sobol' index estimates associated with each of those components, for both algorithms. While there were no difference between the three algorithms for total index estimates associated with the intrinsic noise  $Z$  as a whole (see the bottom of Figure 5), the analysis by type of transition reveals that the total sensitivity estimates of its components significantly differ from one algorithm to the other (see the bottom of Figure 6).

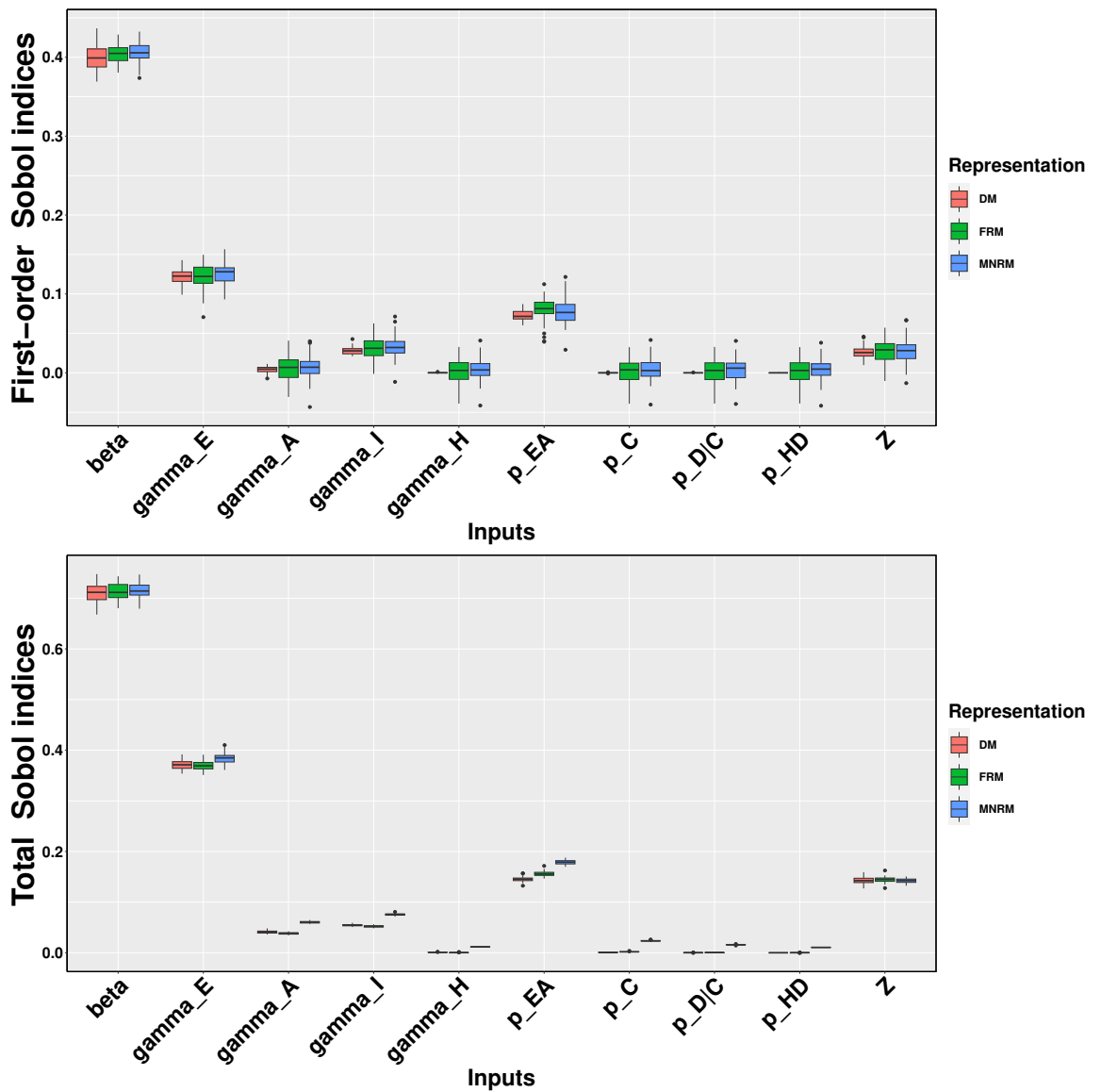


Figure 5: Aggregated (top) first-order and (bottom) total Sobol' index estimates for  $Y_I^\theta$ . For each input parameter (x-axis), boxplots are displayed for each simulation algorithm: (red, left) Gillespie Direct Method, (green, middle) Gillespie First Reaction, (blue, right) Modified Next Reaction. Each boxplot represents 50 independent index estimates, each of them computed with two independent designs of  $n = 2000$  input-output samples.

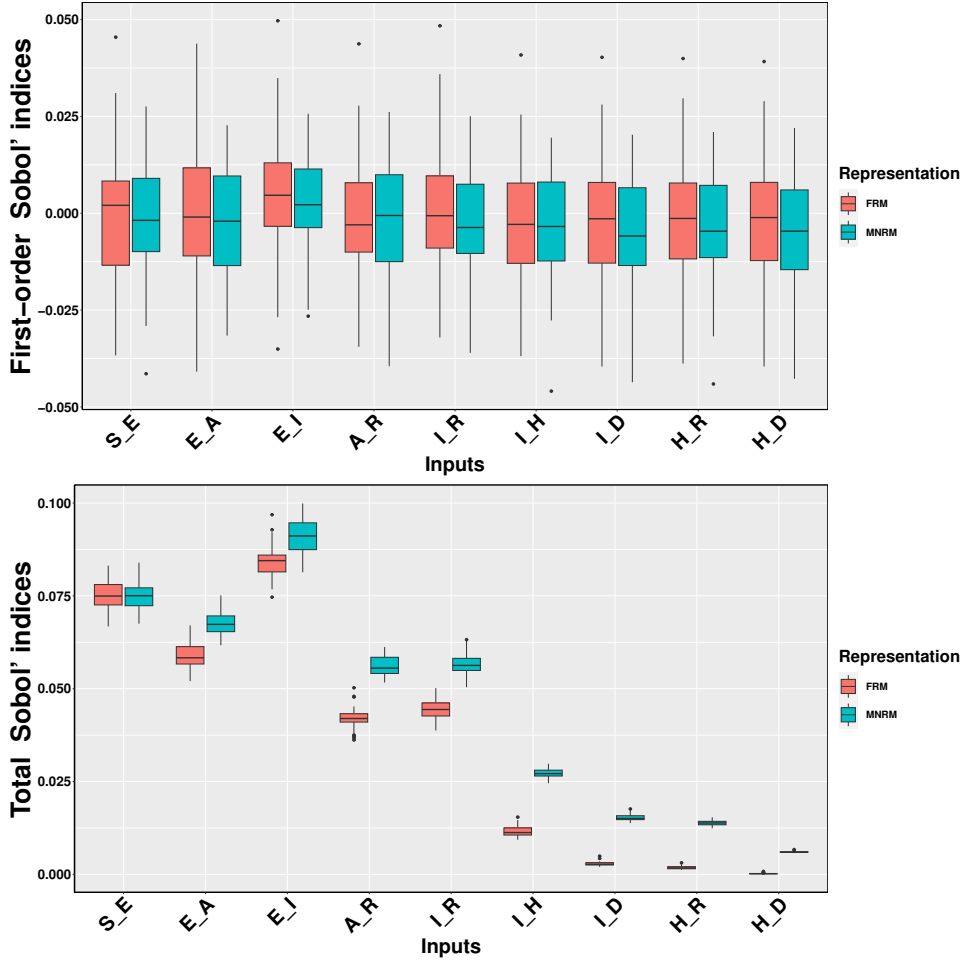


Figure 6: Aggregated (top) first-order and (bottom) total (b) Sobol' indices associated to each component of  $Z$  (each type of transition described in Table 1). For each type of transition (x-axis), boxplots are displayed for (red, left) Gillespie First Reaction and (blue, right) Modified Next Reaction. Each boxplot represents 50 independent index estimates, each of them computed with two independent designs of  $n = 2000$  input-output samples.

The mean dynamical evolution of first-order and total Sobol' index estimates is displayed on Figure 7. Each mean is computed from 50 independent repetitions. At the beginning of the epidemic, the number of infected individuals is mostly sensitive to  $Z$ —that is, to random fluctuations inherent to the model. This confirms that intrinsic randomness rules the dynamics in the emergence phase of an epidemic disease. While the epidemic evolves, the main effect of  $Z$  quickly drops and some uncertain parameters—namely,  $\beta$ ,  $\gamma_E$  and to a less extent  $p_{EA}$ —gain more influence. The uncertain parameter  $\beta$ , in particular, becomes much more important than any other input and remains so until the end. Notice that, except  $\beta$ , the main

effect of every input (both the uncertain parameters and intrinsic noise) approaches zero as the epidemic goes to its end, while the opposite is true for total effects. This indicates that interactions become more prevalent near the end of the epidemic.

Although the most salient features of the performed sensitivity analyses are shared between the three algorithms, we do observe some differences in the mean dynamics across the three algorithms. These differences seem to be significant: see Figure 9, where the sampling variability of the dynamics of first-order and total Sobol' index estimates associated to  $p_{EA}$  are displayed with functional boxplots, namely highest density region (HDR) boxplots, obtained by using the R package `rainbow` developed by Hyndman and Shang [2010]. The HDR boxplot is a visualization tool for functional data based on kernel density estimation of the scores associated to the two first principal components of the functional data (see Hyndman [1996] for further details). The picture clearly indicates that the differences in the mean dynamics obtained from the three different algorithms cannot be attributed to sample variability alone. As another example, a zoom in the time  $t = 60$  (see Figure 8) shows significant differences for the total index estimates of the parameters  $\gamma_I, \gamma_H, p_C, p_{DC}$  and  $p_{HD}$ , and to a less extent  $\gamma_1$  and  $p_{EA}$ .

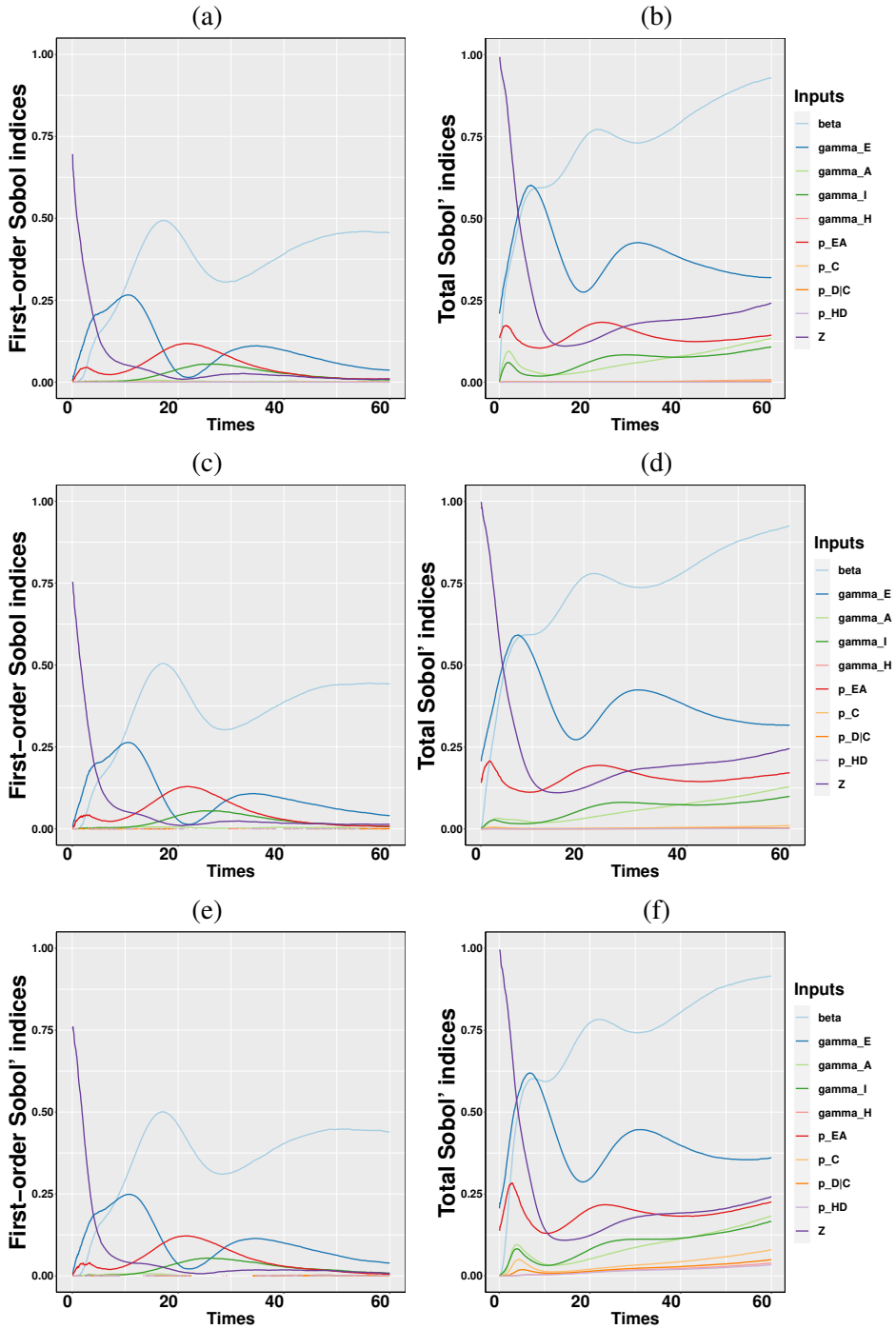


Figure 7: Mean dynamical evolution of (left) first-order and (right) total Sobol' indices for  $Y_I$  with respect to (Figures (a) and (b)) Gillespie Direct Method, (Figure (c) and (d)) Gillespie First Reaction, (Figures (e) and (f)) Modified Next Reaction algorithm. The mean is computed from 50 independent repetitions of the estimation procedure performed with two independent designs of  $n = 2000$  input-output samples.

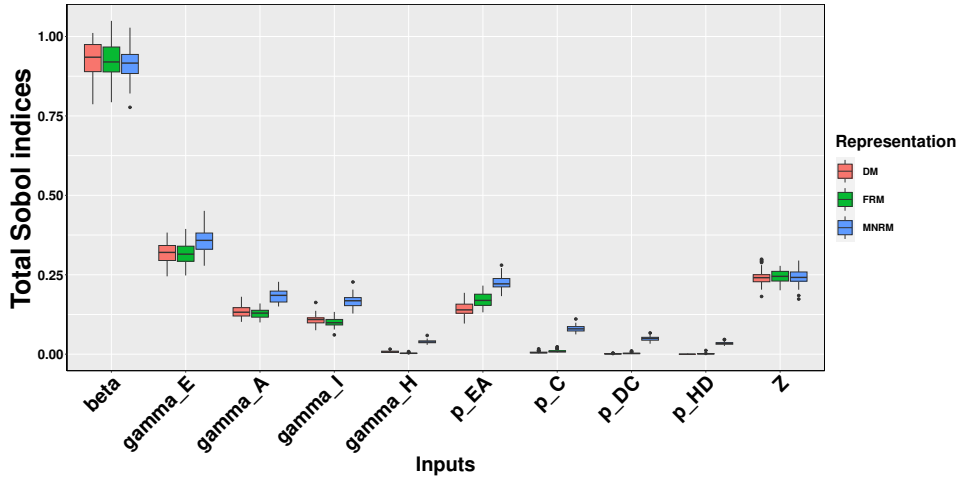


Figure 8: Zoom on total Sobol' indices at time point  $t = 60$ .

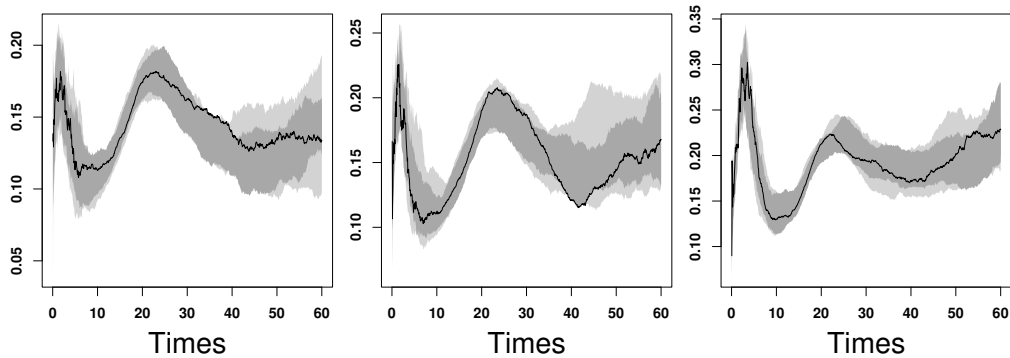


Figure 9: Functional HDR boxplots of dynamical total indices associated to parameter  $p_{E,A}$ , obtained from 50 independent repetitions of the estimation procedure. (left) Gillespie Direct Method, (middle) Gillespie First Reaction Method, (right) Modified Next Reaction Method. The 50 % HDR is plotted in dark gray, the 100 % HDR in light gray and the modal curve, that is the curve in the sample with the highest density is represented by a black solid line.

#### 5.4 Some thoughts about the choice of representations

The numerical experiments confirm that the sensitivity analysis results depend on the choice of the simulation algorithm. An interesting conclusion is that Gillespie algorithms are less prone to interactions between uncertain parameters and intrinsic randomness. It implies that simulations with Gillespie algorithms are more robust to a local perturbation of uncertain input parameters as we can see below by

perturbing parameter  $\beta$ .

To plot Figure 10, we first simulate, for each simulation algorithm (Gillespie Direct Method, Gillespie First Reaction, Modified Next Reaction), 2 000 trajectories (corresponding to 2 000 different seeds) of the difference between the number of symptomatic infectious individuals computed with all uncertain parameters fixed to their nominal value and the number of symptomatic infectious individuals computed by perturbing only parameter  $\beta$  by 5 % from its nominal value. Then in Figure 10 are plotted highest density region (HDR) boxplots.

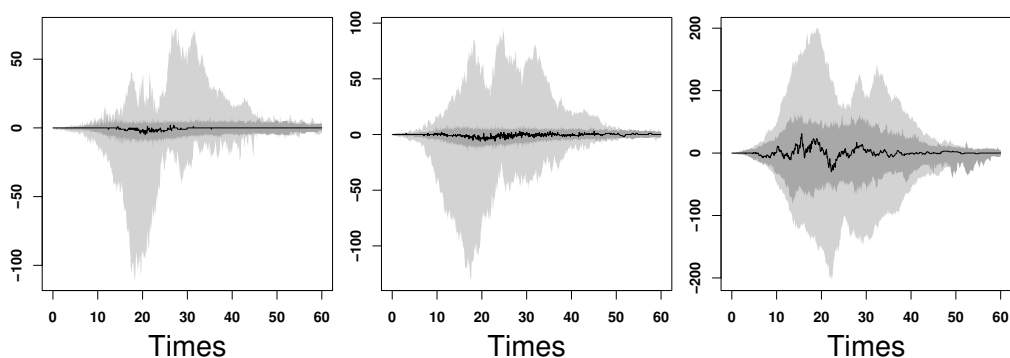


Figure 10: Functional HDR boxplots of differences of the dynamical number of symptomatic infectious individuals computed with uncertain parameters fixed to their nominal value and by perturbing parameter  $\beta$  by 5% from its nominal value: (left) Gillespie Direct Method, (middle) Gillespie First Reaction Method, (right) Modified Next Reaction Method. The 50 % HDR is plotted in dark gray, the 100 % HDR in light gray and the modal curve, that is the curve in the sample with the highest density is represented by a black solid line. Functional HDR boxplots were drawn from 2 000 independent realizations.

## 6 Conclusion

In this work, we proposed a methodology for global sensitivity analysis of stochastic compartmental models described by continuous-time Markov chains. This approach consists in leveraging exact simulation algorithms of the continuous-time Markov chain to propose a representation of the stochastic compartmental model as a deterministic function of the uncertain parameters and controlled latent variables modeling intrinsic randomness. Our study takehome message is that sensitivity analysis results depend on the choice of the representation, which, therefore, must be made with caution and guided by the practitioners' expertise. We exhibited three different representations for CTMC compartmental models, based respectively on Gillespie Direct Algorithm, Gillespie First Reaction Method and Modified Next

Reaction Method. Gillespie Direct Algorithm is computationally advantageous but cannot provide a sensitivity analysis by type of transition, contrarily to Gillespie First Reaction and Modified Next Reaction algorithms. We found that Gillespie Direct algorithm and Gillespie First Reaction algorithm are more robust to local perturbations of the uncertain parameters. We applied our approach to a stochastic compartmental model of SARS-CoV-2 spread.

In the present paper, we considered Markovian models only. However an interesting follow-up would be to extend our results to non-Markovian stochastic processes by using Sellke's construction (Sellke [1983]).

## Declaration

Declarations of interest: none.

## References

- D. F. Anderson. A modified next reaction method for simulating chemical systems with time dependent propensities and delays. *The Journal of Chemical Physics*, 127(21):214107, 2007. doi: 10.1063/1.2799998.
- P. Bittihn and R. Golestanian. Stochastic effects on the dynamics of an epidemic due to population subdivision. *Chaos: An Interdisciplinary Journal of Nonlinear Science*, 30(10):101–102, Oct. 2020. ISSN 1054-1500. doi: 10.1063/5.0028972.
- F. Brauer. *Compartmental Models in Epidemiology*, pages 19–79. Springer Berlin Heidelberg, Berlin, Heidelberg, 2008. ISBN 978-3-540-78911-6. doi: 10.1007/978-3-540-78911-6\_2.
- T. Britton. Stochastic epidemic models: a survey. *Mathematical biosciences*, 225 1:24–35, 2009.
- B. Cazelles, C. Champagne, B. Nguyen-Van-Yen, C. Comiskey, E. Vergu, and B. Roche. A mechanistic and data-driven reconstruction of the time-varying reproduction number: Application to the covid-19 epidemic. *PLOS Computational Biology*, 17(7):1–20, 07 2021. doi: 10.1371/journal.pcbi.1009211.
- A. Courcoul, H. Monod, M. Nielen, D. Klinkenberg, L. Hogerwerf, F. Beaudeau, and E. Vergu. Modelling the effect of heterogeneity of shedding on the within herd coxiella burnetii spread and identification of key parameters by sensitivity analysis. *Journal of Theoretical Biology*, 284(1):130–141, 2011. ISSN 0022-5193. doi: <https://doi.org/10.1016/j.jtbi.2011.06.017>.
- L. Cristancho Fajardo, P. Ezanno, and E. Vergu. Accounting for farmers' control decisions in a model of pathogen spread through animal trade. *Scientific Reports*, 11(1):9581, May 2021. ISSN 2045-2322. doi: 10.1038/s41598-021-88471-6.

- S. Da Veiga, F. Gamboa, B. Iooss, and C. Prieur. *Basics and trends in sensitivity analysis: Theory and practice in R*. SIAM, 2021.
- D. Dupuy, C. Helbert, and J. Franco. DiceDesign and DiceEval: Two R packages for design and analysis of computer experiments. *Journal of Statistical Software*, 65(11):1–38, 2015.
- S. N. Ethier and T. G. Kurtz. *Markov processes – characterization and convergence*, chapter 4, 6. Wiley Series in Probability and Mathematical Statistics: Probability and Mathematical Statistics. John Wiley & Sons Inc., New York, 1986. ISBN 0-471-08186-8.
- P. Étoré, C. Prieur, D. K. Pham, and L. Li. Global sensitivity analysis for models described by stochastic differential equations. *Methodology and Computing in Applied Probability*, 22(2):803–831, June 2020. ISSN 1387-5841, 1573-7713. doi: 10.1007/s11009-019-09732-6.
- J.-C. Fort, T. Klein, and A. Lagnoux. Global sensitivity analysis and Wasserstein spaces. *SIAM/ASA Journal on Uncertainty Quantification*, 9(2):880–921, 2021. doi: 10.1137/20M1354957.
- F. Gamboa, A. Janon, T. Klein, and A. Lagnoux. Sensitivity analysis for multidimensional and functional outputs. *Electronic Journal of Statistics*, 8(1):575 – 603, 2014. doi: 10.1214/14-EJS895.
- D. T. Gillespie. A general method for numerically simulating the stochastic time evolution of coupled chemical reactions. *Journal of Computational Physics*, 22(4):403–434, 1976. ISSN 0021-9991. doi: [https://doi.org/10.1016/0021-9991\(76\)90041-3](https://doi.org/10.1016/0021-9991(76)90041-3).
- S. Goel, S. K. Bhatia, J. P. Tripathi, S. Bugalia, M. Rana, and V. P. Bajiya. SIRC epidemic model with cross-immunity and multiple time delays. *Journal of Mathematical Biology*, 87(3):42, 2023.
- K. Hanthanan Arachchilage, M. Y. Hussaini, N. Cogan, and M. H. Cortez. Exploring how ecological and epidemiological processes shape multi-host disease dynamics using global sensitivity analysis. *Journal of Mathematical Biology*, 86(5):83, 2023.
- J. L. Hart, A. Alexanderian, and P. A. Gremaud. Efficient computation of Sobol’ indices for stochastic models. *SIAM Journal on Scientific Computing*, 39(4): A1514–A1530, 2017. doi: 10.1137/16M106193X.
- W. Hoeffding. A Class of Statistics with Asymptotically Normal Distribution. *The Annals of Mathematical Statistics*, 19(3):293 – 325, 1948. doi: 10.1214/aoms/1177730196.

- T. Homma and A. Saltelli. Importance measures in global sensitivity analysis of nonlinear models. *Reliability Engineering and System Safety*, 52(1):1–17, 1996. ISSN 0951-8320. doi: [https://doi.org/10.1016/0951-8320\(96\)00002-6](https://doi.org/10.1016/0951-8320(96)00002-6).
- R. J. Hyndman. Computing and graphing highest density regions. *The American Statistician*, 50(2):120–126, 1996.
- R. J. Hyndman and H. L. Shang. Rainbow plots, bagplots, and boxplots for functional data. *Journal of Computational and Graphical Statistics*, 19(1):29–45, 2010.
- B. Iooss, S. Da Veiga, A. Janon, and G. Pujol. *sensitivity: Global Sensitivity Analysis of Model Outputs*, 2021. URL <https://CRAN.R-project.org/package=sensitivity>. R package version 1.24.0.
- M. N. Jimenez, O. P. Le Maître, and O. M. Knio. Nonintrusive polynomial chaos expansions for sensitivity analysis in stochastic differential equations. *SIAM/ASA Journal on Uncertainty Quantification*, 5(1):378–402, Jan. 2017. ISSN 2166-2525. doi: 10.1137/16M1061989.
- S. Karlin and H. M. Taylor. *A second course on stochastic processes*. Academic Press, 1981.
- E. S. Knock, L. K. Whittles, J. A. Lees, P. N. Perez-Guzman, R. Verity, R. G. FitzJohn, K. A. M. Gaythorpe, N. Imai, W. Hinsley, L. C. Okell, A. Rosello, N. Kantas, C. E. Walters, S. Bhatia, O. J. Watson, C. Whittaker, L. Cattarino, A. Boonyasiri, B. A. Djaafara, K. Fraser, H. Fu, H. Wang, X. Xi, C. A. Donnelly, E. Jauneikaite, D. J. Laydon, P. J. White, A. C. Ghani, N. M. Ferguson, A. Cori, and M. Baguelin. Key epidemiological drivers and impact of interventions in the 2020 sars-cov-2 epidemic in england. *Science Translational Medicine*, 13(602): 42–62, 2021. doi: 10.1126/scitranslmed.abg4262.
- T. G. Kurtz. Representation and approximation of counting processes. In W. H. Fleming and L. G. Gorostiza, editors, *Advances in Filtering and Optimal Stochastic Control*, pages 177–191, Berlin, Heidelberg, 1982. Springer Berlin Heidelberg. ISBN 978-3-540-39517-1.
- M. Lamboni, M. Hervé, and M. David. Multivariate sensitivity analysis to measure global contribution of input factors in dynamic models. *Reliability Engineering and System Safety*, 96(4):450 – 459, 2011. ISSN 0951-8320. doi: <https://doi.org/10.1016/j.ress.2010.12.002>.
- O. Le Maître and O. Knio. PC analysis of stochastic differential equations driven by wiener noise. *Reliability Engineering & System Safety*, 135:107–124, 2015. ISSN 0951-8320. doi: <https://doi.org/10.1016/j.ress.2014.11.002>.

- O. P. Le Maître, O. M. Knio, and A. Moraes. Variance decomposition in stochastic simulators. *The Journal of Chemical Physics*, 142(24):244115, 2015. doi: 10.1063/1.4922922.
- C. Lin and B. Tang. Latin hypercubes and space-filling designs. In A. Dean, M. Morris, J. Stufken, and D. Bingham, editors, *Handbook of design and analysis of experiments*, Handbooks of modern statistical methods. Chapman & Hall/CRC, 2015.
- S. Marino, I. B. Hogue, C. J. Ray, and D. E. Kirschner. A methodology for performing global uncertainty and sensitivity analysis in systems biology. *Journal of Theoretical Biology*, 254(1):178–196, 2008. ISSN 0022-5193. doi: <https://doi.org/10.1016/j.jtbi.2008.04.011>. URL <https://www.sciencedirect.com/science/article/pii/S0022519308001896>.
- A. Marrel, B. Iooss, S. Da Veiga, and M. Ribatet. Global sensitivity analysis of stochastic computer models with joint metamodels. *Statistics and Computing*, 22(3):833–847, May 2012. ISSN 1573-1375. doi: 10.1007/s11222-011-9274-8.
- M. Massard, R. Eftimie, A. Perasso, and B. Saussereau. A multi-strain epidemic model for covid-19 with infected and asymptomatic cases: Application to french data. *Journal of Theoretical Biology*, 545:111117, 2022. ISSN 0022-5193. doi: <https://doi.org/10.1016/j.jtbi.2022.111117>. URL <https://www.sciencedirect.com/science/article/pii/S0022519322001151>.
- G. Mazo. A trade-off between explorations and repetitions for estimators of two global sensitivity indices in stochastic models induced by probability measures. *SIAM/ASA Journal on Uncertainty Quantification*, 9(4):1673–1713, 2021. doi: 10.1137/19M1272706.
- M. Navarro Jimenez, O. P. Le Maître, and O. M. Knio. Global sensitivity analysis in stochastic simulators of uncertain reaction networks. *The Journal of Chemical Physics*, 145(24):244106, 2016. doi: 10.1063/1.4971797.
- C. N. Ngonghala, M. I. Teboh-Ewungkem, and G. A. Ngwa. Persistent oscillations and backward bifurcation in a malaria model with varying human and mosquito populations: implications for control. *Journal of mathematical biology*, 70(7): 1581–1622, 2015.
- R Core Team. *R: A Language and Environment for Statistical Computing*. R Foundation for Statistical Computing, Vienna, Austria, 2021. URL <https://www.R-project.org/>.
- Q. Richard, S. Alizon, M. Choisy, M. T. Sofonea, and R. Djidjou-Demasse. Age-structured non-pharmaceutical interventions for optimal control of covid-19 epidemic. *PLOS Computational Biology*, 17(3):1–25, 03 2021. doi: 10.1371/journal.pcbi.1008776.

- L. Rimbaud, C. Bruchou, S. Dallot, D. R. J. Pleydell, E. Jacquot, S. Soubeyrand, and G. Thébaud. Using sensitivity analysis to identify key factors for the propagation of a plant epidemic. *Royal Society Open Science*, 5(1):171435, 2018. doi: 10.1098/rsos.171435.
- A. Saltelli, K. Chan, and E. M. Scott. *Sensitivity Analysis*. John Wiley & Sons, 2000.
- T. Sellke. On the asymptotic distribution of the size of a stochastic epidemic. *Journal of Applied Probability*, 20(2):390–394, 1983. doi: 10.2307/3213811.
- I. M. Sobol'. Sensitivity analysis for non-linear mathematical models. *Mathematical Modelling and Computational Experiment*, 1:407–414, 1993.
- A. J. Torii, R. Begnini, H. M. Kroetz, O. M. I. Matar, R. H. Lopez, and L. F. F. Miguel. Global sensitivity analysis for mathematical models comparison. *Computational and Applied Mathematics*, 42(8):345, 2023.
- S. D. Veiga. Kernel-based ANOVA decomposition and shapley effects – application to global sensitivity analysis, 2021. arXiv:2101.05487.
- J. Yang, Y. Chen, and F. Xu. Effect of infection age on an SIS epidemic model on complex networks. *Journal of mathematical biology*, 73:1227–1249, 2016.
- X. Zhu and B. Sudret. Global sensitivity analysis for stochastic simulators based on generalized lambda surrogate models. *Reliability Engineering & System Safety*, 214:107815, 2021. ISSN 0951-8320. doi: <https://doi.org/10.1016/j.ress.2021.107815>.
- X. Zhu and B. Sudret. Stochastic polynomial chaos expansions to emulate stochastic simulators. *International Journal for Uncertainty Quantification*, 13(2):31–52, 2023. ISSN 2152-5080.

# First-order Sobol indices

